automation

MDPI

Article

Distributed PI Observer-Based Sensor Fault Estimation in Networked Multi-Agent Systems with Application to Unmanned Ground Vehicles

Jesus A. Vazquez Trejo [1,*], Arturo D. Espinosa Pedroza [1], Emiliano Peña-Chang [1], José F. Guerrero-Castellanos [2], Manuel Adam-Medina [1,*] and Juan A. Vazquez Trejo [1]

[1] Electronic Engineering Department, TecNM/Centro Nacional de Investigación y Desarrollo Tecnológico (CENIDET), Street Interior Internado Palmira S/N, Col. Palmira, Cuernavaca 62490, Morelos, Mexico; d22ce059@cenidet.tecnm.mx (A.D.E.P.); m25ce031@cenidet.tecnm.mx (E.P.-C.); vtjuan@cenidet.tecnm.mx (J.A.V.T.)

[2] Facultad de Ciencias de la Electrónica, Benemérita Universidad Autónoma de Puebla (BUAP), Ciudad Universitaria, Puebla 72570, Puebla, Mexico; fermi.guerrero@correo.buap.mx

* Correspondence: d18ce045@cenidet.tecnm.mx (J.A.V.T.); manuel.am@cenidet.tecnm.mx (M.A.-M.)

Abstract

This paper addresses the problem of distributed sensor fault estimation (FE) in leader-following multi-agent systems (MASs) composed of unmanned ground vehicles (UGVs). In consensus-based formation control, sensor faults affect the local measurements exchanged among neighboring agents, degrading state estimation and compromising the tracking performance of the entire fleet. Although fault estimation techniques have been widely investigated, most existing distributed formulations do not explicitly address sensor FE within a leader-following consensus framework. A distributed Proportional–Integral (PI) observer is proposed to simultaneously reconstruct the agents' states and estimate sensor fault signals using local and neighbor information. The observer and the leader-following consensus controller are considered within a unified design framework, and sufficient conditions for the simultaneous synthesis of the observer and consensus-controller gains are derived in terms of linear matrix inequalities (LMIs). The proposed methodology is validated through a cooperative UGV formation scenario, where simulation results demonstrate the ability of the distributed observer to reconstruct sensor fault signals and illustrate the effect of sensor faults on the leader-following tracking performance. The proposed approach focuses on sensor fault estimation and does not incorporate an active fault compensation mechanism.

Keywords: multi-agent systems; unmanned ground vehicle; consensus control; fault estimation; sensor faults

Check for updates

Academic Editor: Hefu Ye

Received: 3 September 2026
Revised: 12 October 2026
Accepted: 15 October 2026
Published: 17 October 2026

Copyright: © 2026 by the authors. Licensee MDPI, Basel, Switzerland. This article is an open access article distributed under the terms and conditions of the Creative Commons Attribution (CC BY) license.

1. Introduction

The increasing autonomy of networked systems has enabled multiple agents to cooperate in tasks that are difficult to accomplish with a single system [1]. By distributing sensing, decision-making, and control among interconnected agents, multi-agent systems offer scalability and robustness advantages that have made them widely used in cooperative transportation, mobile robotics, surveillance, and autonomous vehicle coordination [2,3]. Among the platforms used in these applications, UGVs are particularly common due to their low cost and mechanical simplicity, and constitute the agents considered in this

work [4]. Coordinating a UGV fleet requires each agent to rely solely on local information [5]. Consensus control addresses this by achieving agreement among agents through neighbor-to-neighbor information exchange; in leader-following consensus, a leader defines a reference behavior that followers are designed to track using local and neighbor information [6,7]. This distributed structure improves scalability, but also makes cooperative performance strongly dependent on the reliability of each agent's information, since a measurement anomaly at one agent can propagate through the network and degrade the tracking performance of the formation. Fault detection and isolation (FDI) and FE address this vulnerability by identifying faulty components and reconstructing the corresponding fault signals, with applications ranging from aerial robots [8] to unmanned aerial vehicles [9] and intelligent ground vehicles [10]. Model-based observers are widely used for this purpose, including augmented-state [11], Bayesian [12], interval [13], and descriptor-based [14] formulations. Distributed extensions allow local observers to exchange information with neighbors, exploiting collective observability [15,16] by means of intermediate [17,18], unknown-input [19], sliding-mode [20], and adaptive [21] observer structures. However, most of these distributed observer approaches have been developed for single or interconnected systems, without explicitly considering the leader-following consensus setting. Among the various fault types that can affect multi-agent systems, sensor faults are particularly critical. Unlike actuator faults, which affect control actions, sensor faults affect the measurements used for estimation and control. They can manifest as biases, drifts, intermittent readings, or complete outages, typically due to aging, calibration errors, or harsh operating conditions [8–10]. In vehicular applications, such faults typically affect position, velocity, and orientation measurements, which are essential for coordinated operation. A degraded measurement at a single UGV may propagate through the network, compromising the formation-tracking performance of the entire fleet. PI observers offer an attractive structure for simultaneous state and fault reconstruction and have been used in distributed leader-following multi-agent systems for actuator FE [22]. However, sensor faults affect the measured outputs rather than the system dynamics, requiring a reformulation of the observer and its associated error dynamics to extend the proposed framework. Although related sensor FE strategies have been reported for multi-agent systems [23,24], differences in system representations, fault assumptions, and observer structures make a direct quantitative comparison non-straightforward. To address this gap, we propose a distributed sensor FE methodology for leader-following linear time-invariant (LTI) MASs composed of a team of UGVs. The proposed framework considers the distributed PI observer and the leader-following consensus controller within a unified design formulation, allowing the simultaneous synthesis of the observer and controller gains. The estimated fault signal is used for fault reconstruction and is not incorporated into the control law for active fault compensation. This work presents two main contributions. First, a distributed PI observer is developed for simultaneous state and sensor fault estimation, explicitly accounting for sensor faults. Second, the fault estimation dynamics are integrated into the leader-following consensus framework, enabling the joint analysis of state estimation, sensor fault estimation, and consensus tracking. Furthermore, LMI-based sufficient conditions are derived to jointly compute the distributed observer and consensus-controller gains within a unified LMI framework. The remainder of this paper is organized as follows. Section 2 formulates the sensor FE and leader-following consensus problem for LTI multi-agent systems. Section 3 develops the proposed distributed PI observer and derives the conditions for simultaneous state and sensor FE. Section 4 introduces the UGV model considered for validation. Section 5 presents and discusses the simulation results. Finally, Section 6 summarizes the main conclusions of this work.

Preliminaries

Let us consider a directed graph $\mathcal{G}(\mathcal{V}, \mathcal{E}, \mathcal{A})$ where $\mathcal{V} = \{v_1, v_2, \ldots, v_N\}$ is a set of nodes (agents), $\mathcal{E} = \{(i,j) : i,j \in \mathcal{V}\} \subseteq \mathcal{V} \times \mathcal{V}$ is a set of edges, and the adjacency matrix $\mathcal{A} = [a_{ij}] \in \mathbb{R}^{N\times N}$ is defined as $a_{ii} = 0$, $a_{ij} > 0$ if and only if the pair $(i,j) \in \mathcal{E}$; otherwise $a_{ij} = 0$. When the graph is undirected, also, $a_{ij} = a_{ji}$, $\forall i \neq j$ and $\mathcal{A} = \mathcal{A}^T$. The Laplacian matrix $\mathcal{L} \in \mathbb{R}^{N\times N}$ is defined as $\mathcal{L}_{ii} = \sum_{j\neq i} a_{ij}$ and $\mathcal{L}_{ij} = -a_{ij}$. The set of neighbors related to the i-th agent is denoted as $j \in \mathcal{N}_i$. α_i is related with the leader and $\alpha_i = 1$ if there is a link between the i-th agent and the leader; otherwise $\alpha_i = 0$. Defining $\Lambda = diag(\alpha_1, \alpha_2, \ldots, \alpha_N)$, the complete leader-following communication topology can be expressed as $\bar{\mathcal{L}} = \mathcal{L} + \Lambda$, where $\lambda_j(\bar{\mathcal{L}})$, $j = 1, 2, \ldots, N$, denotes the eigenvalues of the communication graph.

Lemma 1 ([25]). *Let X and Y be matrices of compatible dimensions. For any nonsingular matrix S and any scalar $\mu > 0$, the following inequality holds:*

$$X^TY + Y^TX \leq \mu X^TSX + \mu^{-1}Y^TS^{-1}Y.$$

Lemma 2 ([26]). *Consider the symmetric matrix:*

$$\begin{bmatrix} \mathcal{A} & \mathcal{B} \\ \mathcal{B}^T & \mathcal{C} \end{bmatrix} < 0.$$

Then, the following two conditions are equivalent:

$\mathcal{A} < 0, \mathcal{C} - \mathcal{B}^T\mathcal{A}^{-1}\mathcal{B} < 0,$
$\mathcal{C} < 0, \mathcal{A} - \mathcal{B}^T\mathcal{C}^{-1}\mathcal{B} < 0.$

2. Problem Statement

Consider the following homogeneous multi-agent system subject to sensor faults affecting each agent:

$$\begin{aligned} \dot{x}_i(t) &= Ax_i(t) + Bu_i(t), \\ y_i(t) &= Cx_i(t) + S\delta_i(t), \end{aligned} \tag{1}$$

where the subscript i indicates the i-th agent, and N is the total number of agents in the system ($i = 1, 2, \ldots, N$); $x_i(t) \in \mathbb{R}^n$, $u_i(t) \in \mathbb{R}^r$, $y_i(t) \in \mathbb{R}^p$, and $\delta_i(t) \in \mathbb{R}^s$, are the state vector, input vector, output vector, and sensor fault vector, respectively; $A \in \mathbb{R}^{n\times n}$, $B \in \mathbb{R}^{n\times r}$, $C \in \mathbb{R}^{p\times n}$, and $S \in \mathbb{R}^{p\times s}$ are constant system matrices of appropriate dimensions, and S is the matrix that relates the sensor fault vector $\delta_i(t)$ and the output $y_i(t)$. As shown in [8], the system (1) can be expressed in an equivalent form by considering a new state $q_i(t) \in \mathbb{R}^p$, which represents a filtered version of the output vector $y(t)$ as follows:

$$\dot{q}_i(t) = -A_sq_i(t) + A_sCx_i(t) + A_sS\delta_i(t), \tag{2}$$

where $-A_s \in \mathbb{R}^{p\times p}$ is a stable matrix. Let us consider the following vector:

$$\bar{x}_i = [x_i^T(t) \;\; q_i^T(t)]^T, \tag{3}$$

then, the multi-agent system (1) can be expressed in augmented form as follows:

$$\begin{aligned} \dot{\bar{x}}_i(t) &= \bar{A}\bar{x}_i + \bar{B}u_i(t) + \bar{S}\delta_i, \\ \bar{y}_i(t) &= \bar{C}\bar{x}_i(t), \end{aligned} \tag{4}$$

where $\bar{A} \in \mathbb{R}^{(n+p)\times(n+p)}$, $\bar{B} \in \mathbb{R}^{(n+p)\times r}$, $\bar{C} \in \mathbb{R}^{p\times(n+p)}$, and $\bar{S} \in \mathbb{R}^{(n+p)\times s}$ denote the augmented system matrices, given by:

$$\bar{A} = \begin{bmatrix} A & 0 \\ A_s C & -A_s \end{bmatrix}, \ \bar{B} = \begin{bmatrix} B \\ 0 \end{bmatrix}, \ \bar{C} = \begin{bmatrix} 0 & I_p \end{bmatrix}, \ \bar{S} = \begin{bmatrix} 0 \\ A_s S \end{bmatrix}. \tag{5}$$

From the augmented multi-agent system (4), sensor faults can be equivalently treated as actuator faults. It is worth observing that the output is now free of additive fault terms. Moreover, observability of the pair $(\bar{A}, \bar{C})$ is preserved if (A, C) is observable. A distributed Proportional–Integral observer is proposed to achieve the simultaneous estimation of the states of the augmented multi-agent system given in (4) and the sensor faults, as follows:

$$\begin{aligned} \dot{\hat{\chi}}_i(t) &= \bar{A}\hat{\chi}_i(t) + \bar{B}u_i(t) + G_P(\bar{C}\bar{x}_i(t) - \bar{C}\hat{\chi}_i(t)) + \bar{S}\hat{\delta}_i(t), \\ \dot{\hat{\delta}}_i(t) &= G_I(\bar{C}\bar{x}_i(t) - \bar{C}\hat{\chi}_i(t)), \\ \hat{y}_i(t) &= \bar{C}\hat{\chi}_i(t), \end{aligned} \tag{6}$$

where $\hat{\chi}_i(t) \in \mathbb{R}^{(n+p)}$ denotes the estimated state vector, $\hat{\delta}_i(t) \in \mathbb{R}^s$ is the estimate of the fault, and $\hat{y}_i(t) \in \mathbb{R}^p$ is the observer output. The matrices $G_P \in \mathbb{R}^{(n+p)\times p}$ and $G_I \in \mathbb{R}^{s\times p}$ are the proportional and integral gains to be designed, respectively. Defining the estimation error as $e_i(t) = \bar{x}_i(t) - \hat{\chi}_i(t)$, the dynamics of the estimation error are:

$$\dot{e}_i(t) = (\bar{A} - G_P\bar{C})e_i(t) + \bar{S}\zeta_i(t), \tag{7}$$

where $\zeta_i(t) = \delta_i(t) - \hat{\delta}_i(t)$ is the FE error. Differentiating $\zeta_i(t)$ and assuming $\dot{\delta}_i(t) = 0$, $\dot{\zeta}_i(t)$ can be written as:

$$\dot{\zeta}_i(t) = -\dot{\hat{\delta}}_i(t) = -G_I(\bar{C}\bar{x}_i(t) - \bar{C}\hat{\chi}_i(t)). \tag{8}$$

Defining a new error vector $\epsilon_i(t) = [e_i^T(t), \ \zeta_i^T(t)]^T \in \mathbb{R}(n+p+s)$ (7) and (8) can be expressed as follows:

$$\dot{\epsilon}_i(t) = (\tilde{A} - \tilde{G}\tilde{C})\epsilon_i(t), \tag{9}$$

where

$$\tilde{A} = \begin{bmatrix} \bar{A} & \bar{S} \\ 0 & 0 \end{bmatrix}, \ \tilde{G} = \begin{bmatrix} G_P \\ G_I \end{bmatrix}, \ \tilde{C} = \begin{bmatrix} \bar{C} & 0 \end{bmatrix}. \tag{10}$$

The control objective of the multi-agent system is to track the reference trajectories established by a virtual leader, which are of the form:

$$\dot{x}_l(t) = Ax_l(t), \tag{11}$$

where $x_l(t) \in \mathbb{R}^n$ is the state vector of the virtual leader. Let the synchronization error between each follower and the virtual leader be defined as $\xi_i(t) = x_i(t) - x_l(t)$, then, the dynamics of the synchronization error between each i-th agent and the virtual leader is:

$$\dot{\xi}_i(t) = A\xi_i(t) + Bu_i(t). \tag{12}$$

Proposing the following observer-based consensus protocol:

$$u_i(t) = K\Big[a_{ij}\big(\hat{x}_i(t) - \hat{x}_j(t)\big) + \alpha_i\big(\hat{x}_i(t) - x_l(t)\big)\Big], \tag{13}$$

where $\hat{x}_i(t) \in \mathbb{R}^n$ is the estimation state vector of (1), $\hat{x}_j(t)$ are the estimated state vector of the neighbors of the i-th agent, and $K \in \mathbb{R}^{r\times n}$ represents the control gain to be designed, with the objective to guarantee that the followers track the virtual leader. It is worth noting

that $\hat{x}_i(t)$ is a component of the augmented state $\hat{\chi}_i(t)$, therefore, the following expression is defined by means of the extraction matrix Π, as shown below:

$$\hat{x}_i(t) = \Pi\hat{\chi}_i(t), \;\; \Pi = \begin{bmatrix} I_n & 0_{n\times p} \end{bmatrix} \in \mathbb{R}^{n\times(n+p)}. \tag{14}$$

3. Fault Estimation Observer-Based Leader-Following Consensus Control for Multi-Agent Systems

By substituting the consensus protocol (13) into (12), employing the Kronecker product, the vectors $\xi(t) = [\xi_1^T(t),\, \xi_2^T(t), \ldots,\, \xi_N^T(t)]^T$, and $\epsilon(t) = [\epsilon_1^T(t),\, \epsilon_2^T(t), \ldots,\, \epsilon_N^T(t)]^T$ both the estimation error and the synchronization error equations can be expressed in compact form as:

$$\dot{\xi}(t) = (I_N \otimes A + \bar{\mathcal{L}} \otimes BK)\xi(t) - (\bar{\mathcal{L}} \otimes BK)\epsilon(t), \tag{15}$$

$$\dot{\epsilon}(t) = I_N \otimes (\tilde{A} - \tilde{G}\tilde{C})\epsilon(t). \tag{16}$$

By introducing a new vector $\kappa(t) = [\xi^T(t),\, \epsilon^T(t)]^T$, the errors can be rewritten so as to define the closed-loop multi-agent system.

$$\dot{\kappa}(t) = \begin{bmatrix} \dot{\xi}(t) \\ \dot{\epsilon}(t) \end{bmatrix} = \begin{bmatrix} (I_N \otimes A + \bar{\mathcal{L}} \otimes BK) & -(\bar{\mathcal{L}} \otimes BK\Pi_\epsilon) \\ 0 & I_N \otimes (\tilde{A} - \tilde{G}\tilde{C}) \end{bmatrix} \begin{bmatrix} \xi(t) \\ \epsilon(t) \end{bmatrix}, \tag{17}$$

where $\Pi_\epsilon = [\Pi,\, 0_{n\times s}] \in \mathbb{R}^{n\times(n+p+s)}$ denotes the augmented extraction matrix. The following theorem provides LMI-based conditions that guarantee the existence of the control and observer gains based on the Lyapunov stability analysis.

Theorem 1. *Let the multi-agent system in closed loop* (17) *be considered. The synchronization errors* (15) *together with the estimation errors* (16) *converge exponentially, for every eigenvalue* $\lambda_j(\bar{\mathcal{L}})$*, there exist symmetric positive-definite matrices* $\bar{P}_1 \in \mathbb{R}^{n\times n}$ *and* $P_2 \in \mathbb{R}^{(n+p+s)\times(n+p+s)}$*, matrices R and M of appropriate dimensions, and a positive scalar* ρ*, satisfying the matrix inequality*

$$\begin{bmatrix} \mathcal{Q}_{j_{11}} & 0 & \mathcal{Q}_{j_{13}} & 0 \\ * & \mathcal{Q}_{22} & 0 & \Pi_\epsilon^T \\ * & * & -\rho^{-1}\bar{P}_1 & 0 \\ * & * & * & -\rho\bar{P}_1 \end{bmatrix} < 0, \tag{18}$$

with $\mathcal{Q}_{j_{11}} = He\{A\bar{P}_1 + \lambda_j BR\}$, $\mathcal{Q}_{22} = He\{P_2\tilde{A} - M\tilde{C}\}$, *and* $\mathcal{Q}_{j_{13}} = -\lambda_j BR$. *Under these conditions, the controller and observer gains are respectively recovered as* $K = R\bar{P}_1^{-1}$ *and* $\tilde{G} = P_2^{-1}M$.

Proof of Theorem 1. Consider the following quadratic Lyapunov function candidate:

$$V(\kappa) = \begin{bmatrix} \xi^T(t) & \epsilon^T(t) \end{bmatrix} \begin{bmatrix} I_N \otimes P_1 & 0 \\ 0 & I_N \otimes P_2 \end{bmatrix} \begin{bmatrix} \xi(t) \\ \epsilon(t) \end{bmatrix}, \tag{19}$$

where $P_1 \in \mathbb{R}^{n\times n}$ and $P_2 \in \mathbb{R}^{(n+p+s)\times(n+p+s)}$ are symmetric matrices. The symbol $*$ signifies the symmetric elements of a matrix. Along the trajectories of (17), the derivative of the Lyapunov function is provided by (the time dependence is removed for simplicity):

$$\begin{aligned} \dot{V}(\kappa) = &\begin{bmatrix} \xi^T & \epsilon^T \end{bmatrix} \begin{bmatrix} I_N \otimes P_1 & 0 \\ 0 & I_N \otimes P_2 \end{bmatrix} \\ &\times \begin{bmatrix} I_N \otimes A + \overline{\mathcal{L}} \otimes BK & \left(-\overline{\mathcal{L}} \otimes BK\Pi_\epsilon\right) \\ 0 & I_N \otimes \left(\tilde{A} - \tilde{G}\tilde{C}\right) \end{bmatrix} \begin{bmatrix} \xi \\ \epsilon \end{bmatrix}. \end{aligned} \tag{20}$$

$$\begin{aligned}\dot{V}(\kappa) =& 2\xi^T\big(I_N \otimes P_1 A + \overline{\mathcal{L}} \otimes P_1 BK\big)\xi \\ &+ 2\xi^T(I_N \otimes P_1)\big(-\overline{\mathcal{L}} \otimes BK\Pi_\epsilon\big)\epsilon + 2\epsilon^T\big(I_N \otimes P_2\big(\tilde{A} - \tilde{G}\tilde{C}\big)\big)\epsilon.\end{aligned} \tag{21}$$

As the communication graph is undirected, the Laplacian matrix $\mathcal{L}$ is symmetric. Moreover, since Λ is diagonal, the leader-pinned Laplacian matrix $\bar{\mathcal{L}} = \mathcal{L} + \Lambda$ is also symmetric. Under the assumption that at least one follower is connected to the leader, $\bar{\mathcal{L}}$ is positive definite. Therefore, by the spectral theorem, there exists an orthogonal matrix $T \in \mathbb{R}^{N\times N}$ such that $T^T\bar{\mathcal{L}}T = J$, $J = \mathrm{diag}(\lambda_1, \lambda_2, \ldots, \lambda_N)$, where $\lambda_j > 0$, $j = 1, \ldots, N$, and $T^{-1} = T^T$. To consistently apply this transformation to the complete quadratic Lyapunov function, define the new coordinates:

$$\psi = (T^T \otimes I_n)\xi, \qquad \chi = (T^T \otimes I_{n+p+s})\epsilon. \tag{22}$$

Substituting these transformations into the Lyapunov function and using the mixed-product property of the Kronecker product, together with the orthogonality condition $T^TT = I_N$, yields:

$$\begin{aligned}V(\kappa) &= \psi^T(T^T \otimes I_n)(I_N \otimes P_1)(T \otimes I_n)\psi + \chi^T(T^T \otimes I_{n+p+s})(I_N \otimes P_2)(T \otimes I_{n+p+s})\chi \\ &= \psi^T(I_N \otimes P_1)\psi + \chi^T(I_N \otimes P_2)\chi.\end{aligned} \tag{23}$$

Therefore, the quadratic structure of the Lyapunov function is preserved under the orthogonal coordinate transformation. Applying the same transformation consistently to (21), and using $T^T\bar{\mathcal{L}}T = J$, gives:

$$\begin{aligned}\dot{V}(\kappa) =& 2\psi^T(I_N \otimes P_1 A + J \otimes P_1 BK)\psi + 2\psi^T(I_N \otimes P_1)(-J \otimes BK\Pi_\epsilon)\chi \\ &+ 2\chi^T\big[I_N \otimes P_2(\tilde{A} - \tilde{G}\tilde{C})\big]\chi.\end{aligned} \tag{24}$$

Since $J = \mathrm{diag}(\lambda_1, \ldots, \lambda_N)$ is diagonal, the transformed dynamics can be decomposed into N independent modal components associated with the eigenvalues λ_j of $\bar{\mathcal{L}}$. Thus, Equation (24) can be equivalently expressed as:

$$\begin{aligned}\dot{V}(\kappa) =& 2\psi^T\big(I_N \otimes P_1 A + \lambda_j \otimes P_1 BK\big)\psi \\ &+ 2\psi^T(I_N \otimes P_1)\big(-\lambda_j \otimes BK\Pi_\epsilon\big)\chi + 2\chi^T\big(I_N \otimes P_2\big(\tilde{A} - \tilde{G}\tilde{C}\big)\big)\chi.\end{aligned} \tag{25}$$

Considering the vector $\tau = \big[\psi^T, \chi^T\big]^T$, expression (25) can be rewritten as follows:

$$\dot{V}(\kappa) = \tau^T\begin{bmatrix} \mathrm{He}\{P_1A + \lambda_j P_1 BK\} & \big(-\lambda_j P_1 BK\Pi_\epsilon\big) \\ * & He\{P_2\tilde{A} - P_2\tilde{G}\tilde{C}\} \end{bmatrix}\tau, \tag{26}$$

Defining $\bar{P}_1 = P_1^{-1}$ where $\bar{P}_1$ is a symmetric matrix.

$$\begin{bmatrix} \bar{P}_1 & 0 \\ 0 & I_{(n+p+s)} \end{bmatrix}\begin{bmatrix} \mathrm{He}\{\bar{P}_1A + \lambda_j \bar{P}_1 BK\} & \big(-\lambda_j \bar{P}_1 BK\Pi_\epsilon\big) \\ * & He\{P_2\tilde{A} - P_2\tilde{G}\tilde{C}\} \end{bmatrix}\begin{bmatrix} \bar{P}_1 & 0 \\ 0 & I_{(n+p+s)} \end{bmatrix} < 0. \tag{27}$$

Then, the expression (27) can be rewritten as follows:

$$\begin{bmatrix} \mathrm{He}\big(A\bar{P}_1 + \lambda_j BK\bar{P}_1\big) & 0_{n,(n+p+s)} \\ * & \mathrm{He}\big(P_2\tilde{A} - P_2\tilde{G}\tilde{C}\big) \end{bmatrix} + \mathrm{He}\left\{\begin{bmatrix} -\lambda_j BK \\ 0 \end{bmatrix}\begin{bmatrix} 0 & \Pi_\epsilon \end{bmatrix}\right\} < 0. \tag{28}$$

Applying the Young relation (Lemma 1) in (28), the following inequality is obtained:

$$\begin{bmatrix} \mathrm{He}\{A\bar{P}_1 + \lambda_j BK\bar{P}_1\} & 0_{n,(n+p+s)} \\ * & \mathrm{He}\{P_2A - P_2\tilde{G}\tilde{C}\} \end{bmatrix} + \rho \begin{bmatrix} -\lambda_j BK \\ 0 \end{bmatrix} \bar{P}_1 \begin{bmatrix} (-\lambda_j BK)^T & 0 \end{bmatrix} + \rho^{-1} \begin{bmatrix} 0 \\ \Pi_\epsilon \end{bmatrix} \bar{P}_1^{-1} \begin{bmatrix} 0 & \Pi_\epsilon^T \end{bmatrix} < 0, \tag{29}$$

where $\rho > 0$. Employing the Schur complement (Lemma 2), taking into account $R = K\bar{P}_1$, and $M = P_2\tilde{G}$, the proof is completed. □

Remark 1. *For directed graphs, $\bar{\mathcal{L}}$ is no longer symmetric, so the orthogonal decomposition cannot be used and the analysis would rely on the real Jordan form or on a Lyapunov equation based on the graph structure. For switching topologies, the LMI conditions would need to hold for the eigenvalues of every admissible graph, either with a common Lyapunov function or, less conservatively, with multiple Lyapunov functions under a dwell-time condition.*

4. Kinematic Model

4.1. Nonlinear Model

To simplify the geometric representation of the robot system, the original four-wheel configuration is reduced to an equivalent two-wheel model, commonly referred to as the bicycle model [27]. The reference point of the bicycle model is located at the midpoint of the rear axle, and its mathematical representation is given by:

$$\begin{bmatrix} \dot{\mathbf{x}} \\ \dot{\mathbf{y}} \\ \dot{\boldsymbol{\theta}} \end{bmatrix} = \begin{bmatrix} v_x \cos(\theta) \\ v_x \sin(\theta) \\ \frac{v_x}{L} \tan(\phi) \end{bmatrix}, \tag{30}$$

where x and y denote the Cartesian coordinates of the vehicle, v_x is the longitudinal velocity, ϕ is the steering angle, L is the distance between the front and back wheels, and θ is the orientation. The steering angle ϕ can be expressed in a different term to simplify the bicycle model:

$$\phi = \arctan\left(\frac{\omega L}{v_x}\right), \tag{31}$$

where ω denotes the angular velocity of the vehicle or the instantaneous center of rotation (ICR).

The kinematic expression on (30) has a non-holonomic restriction because the coordinate reference is between the rear axle midpoint. To avoid this movement restriction, the coordinate reference is moved along the vehicle on its center of mass P, where the distance between the rear axle midpoint and p is assumed as constant distance l_r, and the state of the system is expressed as: $\mathbf{X} = [\mathbf{x}\ \mathbf{y}\ \boldsymbol{\theta}]^T$. This coordinate configuration is illustrated in Figure 1.

The coordinates of the center of mass P with respect to the initial reference frame E^f, where X_G and Y_G denote the global coordinates along the x- and y-axes, respectively, are given by:

$$X_p = \begin{bmatrix} x_p \\ y_p \end{bmatrix} = \begin{bmatrix} x \\ y \end{bmatrix} + l_r \begin{bmatrix} \cos(\theta) \\ \sin(\theta) \end{bmatrix}. \tag{32}$$

To track the point's motion P over time, we differentiate the new position expressions defined as $\mathbf{x_p} = [x_p\ y_p]$.

$$\dot{\mathbf{x}}_\mathbf{p} = \begin{bmatrix} \dot{x}_p \\ \dot{y}_p \end{bmatrix} = \begin{bmatrix} \cos(\theta) & -l_r \sin(\theta) \\ \sin(\theta) & l_r \cos(\theta) \end{bmatrix} \begin{bmatrix} v_x \\ \omega \end{bmatrix}. \tag{33}$$

The coordinate change (33) determines the next coordinate change:

$$\begin{bmatrix} v_x \\ \omega \end{bmatrix} = \begin{bmatrix} \cos(\theta) & \sin(\theta) \\ -\frac{1}{l_r}\sin(\theta) & \frac{1}{l_r}\cos(\theta) \end{bmatrix} \begin{bmatrix} u_x \\ u_y \end{bmatrix}, \tag{34}$$

where the control vector is defined as $u = [u_x\ u_y]^T$ from the consensus control to track the desired formation.

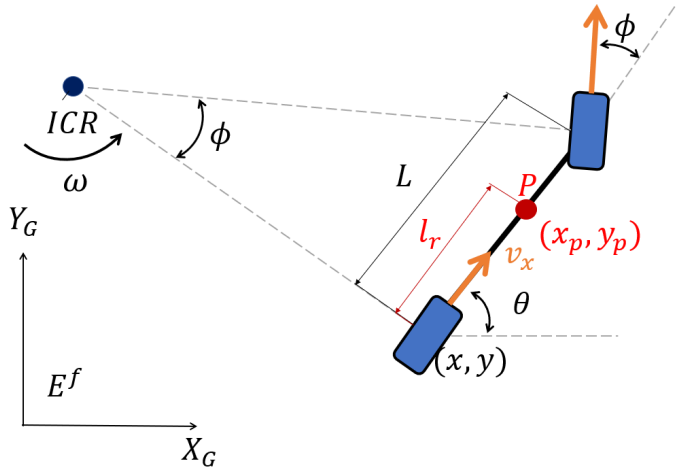

Figure 1. Diagram representing the kinematic bicycle model for car-like mobile robot.

4.2. Linear Model

The state and control vectors are defined as:

$$\mathbf{x_p} = \begin{bmatrix} x_p \\ y_p \end{bmatrix} \in \mathbb{R}^2, \qquad \mathbf{u} = \begin{bmatrix} u_x \\ u_y \end{bmatrix} \in \mathbb{R}^2. \tag{35}$$

Then, the linear model is described in [27]. In terms of these variables, Equation (35) admits the following linear state-space representation:

$$\begin{aligned} \dot{\mathbf{x}} &= \mathbf{A}\mathbf{x} + \mathbf{B}\mathbf{u}, \\ \mathbf{y} &= \mathbf{C}\mathbf{x}, \end{aligned} \tag{36}$$

with

$$\mathbf{A} = \begin{bmatrix} 0 & 0 \\ 0 & 0 \end{bmatrix}, \qquad \mathbf{B} = \begin{bmatrix} 1 & 0 \\ 0 & 1 \end{bmatrix}, \qquad \mathbf{C} = \begin{bmatrix} 1 & 0 \\ 0 & 1 \end{bmatrix}.$$

The pair (A, B) is controllable and (A, C) is observable [27], which guarantees the existence of a stabilizing state-feedback gain and ensures that the state trajectories can be reconstructed from the available output measurements, a necessary condition for the observer-based FE scheme proposed in this work.

5. Simulation Results

This section evaluates the performance of the proposed distributed observer-based sensor FE framework through numerical simulations involving a team of UGVs. The

analysis evaluates the performance of the distributed PI observers in reconstructing system states and estimating sensor faults using locally available measurements and information exchanged among neighboring agents. The simulations evaluate the accuracy of the resulting estimates and their tracking performance during fault occurrences.

Figure 2 illustrates the closed-loop leader-following consensus and sensor FE scheme considered in the simulations. The virtual leader provides the reference trajectory (x_l), which is used by the consensus controller together with the estimated states ($\hat{x}_i$) and ($\hat{x}_j$) to determine the control input (u_i). The control signal is applied to the nonlinear UGV dynamics, while sensor faults (f_{s_i}) affect the corresponding measurements. A distributed PI observer is employed to reconstruct the system states and estimate the sensor fault signals using local measurements and information exchanged with neighboring UGVs. The resulting estimates provide information for monitoring the sensor fault behavior and evaluating the estimation performance of the proposed FE scheme.

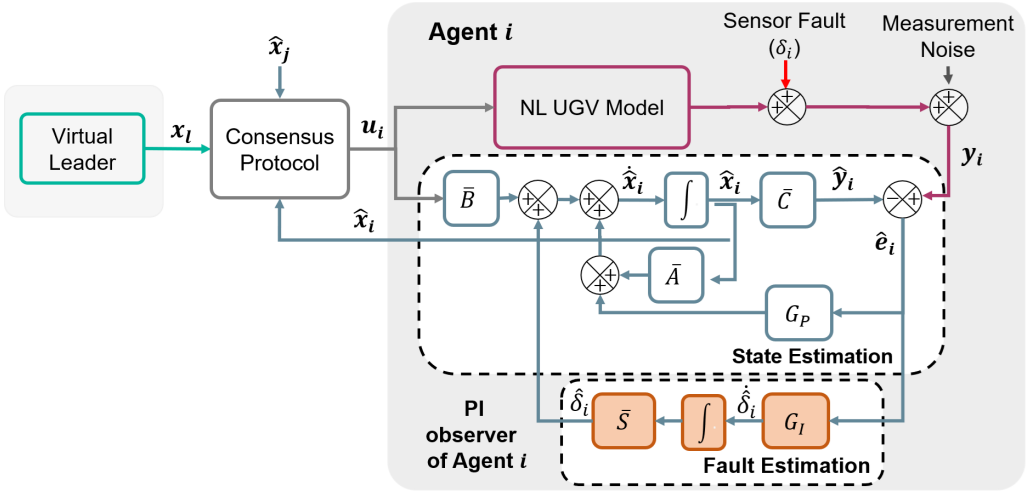

Figure 2. Model-based leader-following consensus control framework for a UGV teams.

For validation purposes, each UGV is represented by the nonlinear model derived from (33). The distributed PI observer is designed to simultaneously reconstruct the system states and estimate sensor fault signals. The estimated states ($\hat{x}_i$) are provided to the consensus controller to overcome the lack of complete state measurements, while the reconstructed sensor fault signals ($\hat{\delta}_i$) provide information about the sensor fault behavior and are used to evaluate the fault estimation performance of the proposed observer.

The communication among the UGVs is described by an undirected graph, as shown in Figure 3. This topology enables the derivation of the information matrices required for the consensus protocol.

The communication matrix associated with the virtual leader is denoted by $\Lambda = diag(1, 0, 0, 0)$. Additionally, the Laplacian matrix $\mathcal{L}$ is given by:

$$\mathcal{L} = \begin{bmatrix} 2 & -1 & 0 & -1 \\ -1 & 2 & -1 & 0 \\ 0 & -1 & 2 & -1 \\ -1 & 0 & -1 & 2 \end{bmatrix}. \tag{37}$$

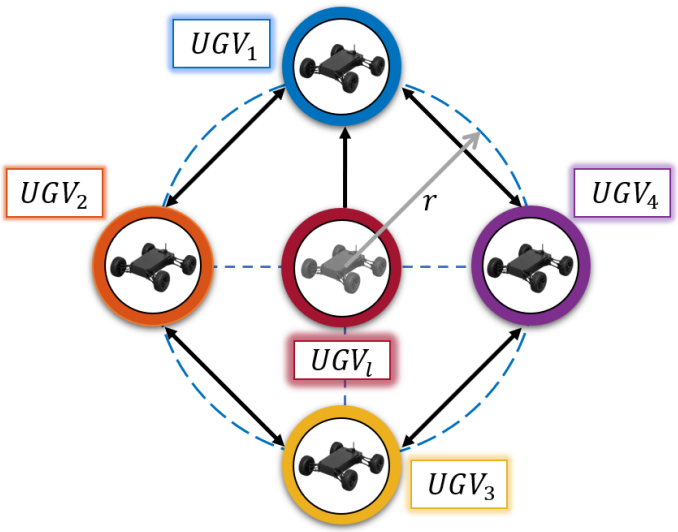

Figure 3. Communication topology between agents.

The agents are arranged in a diamond formation, which is defined by the matrix H. In this simulation, four follower UGVs ($N = 4$) are considered, with the components h_i representing the desired positions along the x and y axes:

$$H = r \cdot \begin{bmatrix} \cos(\theta_l) & \cos(90^\circ + \theta_l) & \cos(180^\circ + \theta_l) & \cos(270^\circ + \theta_l) \\ \sin(\theta_l) & \sin(90^\circ + \theta_l) & \sin(180^\circ + \theta_l) & \sin(270^\circ + \theta_l) \end{bmatrix}, \tag{38}$$

where r denotes the radius of the encompassing circle. The UGVs are positioned at the vertices of a diamond inscribed within this circle, with its center coinciding with the position of the virtual leader. The initial conditions for the UGVs, their corresponding observers, and the virtual leader are summarized in Table 1.

Table 1. Initial conditions of the system and observers.

UGV	x_p [m]	y_p [m]	$\hat{x}_p$ [m]	$\hat{y}_p$ [m]
1	0	2	2	−0.5
2	1	1	−1	−0.5
3	1	−1	2	−0.5
4	0	−2	−1	−0.5
Leader	0	0	-	-

To compute the control gain K and the observer gains G_P and G_I, the LTI representation of the UGVs in (36) is used to obtain a solution to the LMIs presented in Theorem 1 with $\rho = 0.05$. The LMIs were implemented in MATLAB R2018b using YALMIP and solved with the SeDuMi toolbox. The resulting controller and observer gains are given by:

$$K = \begin{bmatrix} -6.75 & 0 \\ 0 & -6.75 \end{bmatrix}, \quad G_P = \begin{bmatrix} 17.02 & 0 \\ 0 & 13.61 \\ 273.06 & 0 \\ 0 & 237.95 \end{bmatrix}, \quad G_I = \begin{bmatrix} 170.40 & 0 \\ 0 & 136.22 \end{bmatrix}. \tag{39}$$

5.1. Nominal Case

The first simulation considers a fault-free operating scenario, in which the UGVs are required to coordinate their motion while tracking the prescribed reference trajectory. The controller and observer gains are fixed at the selected values, and a zero-mean Gaussian noise with a standard deviation of 0.01 $[m]$ is added to the sensor measurements to account

for measurement uncertainties. The resulting motion of the UGVs in the 2D plane is shown in Figure 4.

Figure 5 presents the estimation errors obtained from the observers under fault-free conditions. As can be seen, all errors rapidly converge toward zero, indicating that the observers are able to reconstruct the UGV states with satisfactory accuracy and maintain reliable state estimation throughout the maneuver.

The synchronization error between the virtual leader and each follower is shown in Figure 6, where the synchronization error is defined as $\xi = \|x_i - x_l\| - r$. The error converges to zero, indicating that the followers effectively achieve and maintain synchronization with the leader's position.

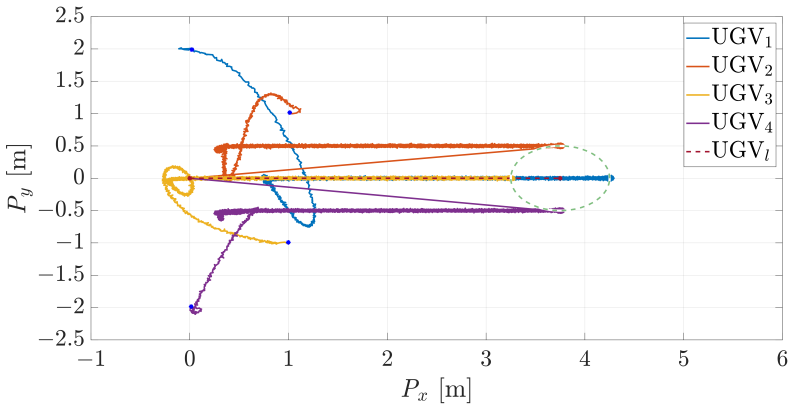

Figure 4. UGV trajectories in the 2D plane under fault-free conditions.

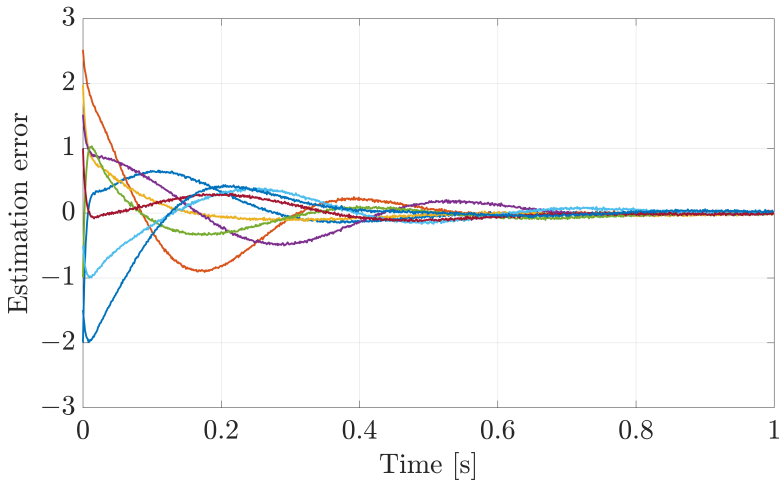

Figure 5. Estimation errors for all observers.

The relative distances between the UGVs during the fault-free scenario are shown in Figure 7. These distances remain constant and close to the predefined values, indicating that the formation is maintained stably throughout the simulation. The formation error for each pair of UGVs is defined as:

$$d_{ij} = \left| \left([x_i, y_i]^T - [x_j, y_j]^T \right) - (h_i - h_j) \right|, \tag{40}$$

where the desired diamond formation is achieved when $d_{ij} = 0$.

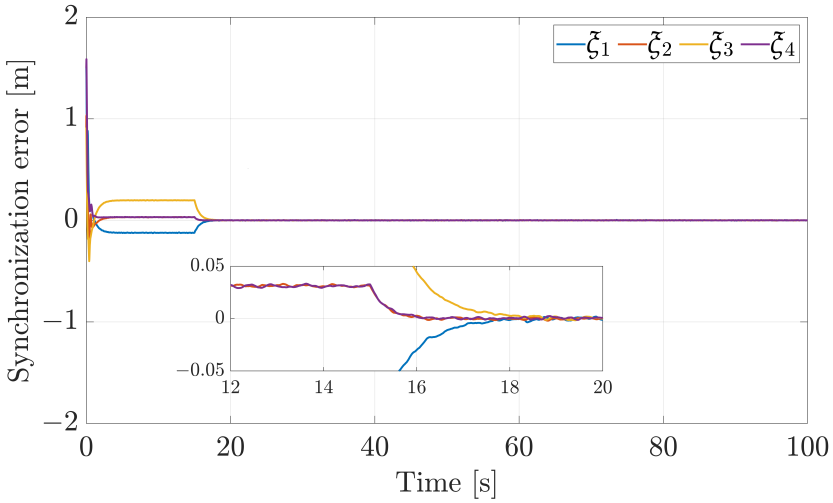

Figure 6. Synchronization error between the leader UGV and the follower agents.

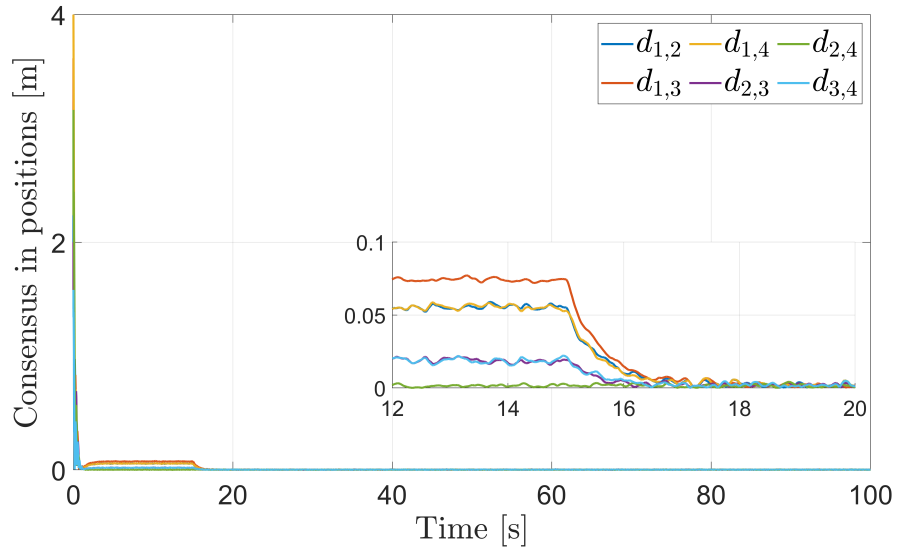

Figure 7. Relative distances among the UGVs.

5.2. Fault Case

To evaluate the performance of the proposed observer under sensor fault conditions, the behavior of the UGV_1 formation is analyzed in the presence of a measurement fault, as shown in Figure 8. Particular attention is given to the accuracy of the FE, since reliable fault reconstruction is essential for characterizing the sensor fault behavior and assessing the performance of the proposed observer. For this purpose, a sensor fault is introduced in UGV_1 during a predefined time interval.

The considered fault is modeled as an additive sensor fault affecting one of the measurements of UGV_1. The fault is intermittent and is activated only within the specified time interval, while the sensor operates normally before and after the fault occurrence. The fault profile is defined as:

$$\delta_1 = \begin{cases} \begin{bmatrix} 0 \\ 0 \end{bmatrix}, & 0\,\text{s} \leq t < 30\,\text{s}; \\ \begin{bmatrix} 0.6\,\text{m}; \\ 0 \end{bmatrix}, & 30\,\text{s} \leq t \leq 60\,\text{s}; \\ \begin{bmatrix} 0 \\ 0 \end{bmatrix}, & t > 60\,\text{s}; \end{cases} \tag{41}$$

where δ_1 represents the magnitude of the sensor fault introduced in UGV_1. The sensor operates under fault-free conditions for $t < 30\,\text{s}$ and is affected by an additive fault during $30\,\text{s} \leq t \leq 60\,\text{s}$. For $t > 60\,\text{s}$, the fault disappears and the sensor returns to its fault-free operation.

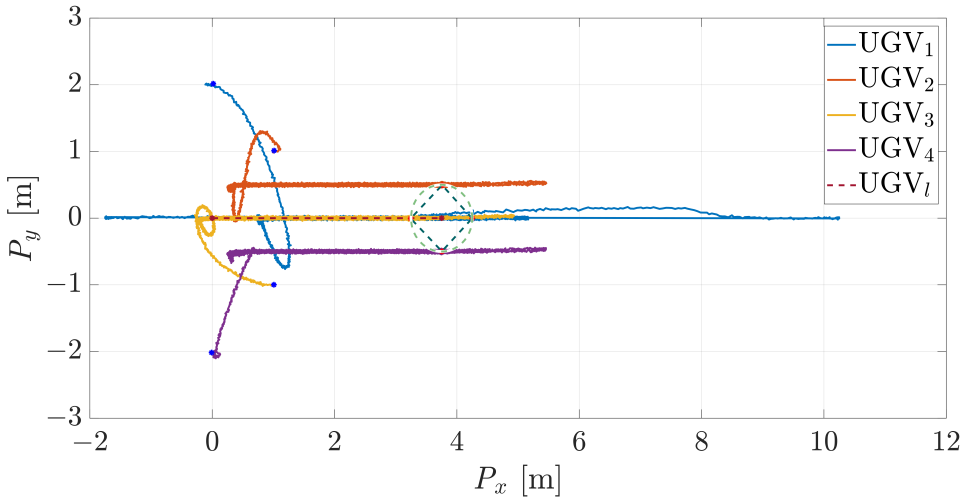

Figure 8. UGV trajectories in the 2D plane under sensor fault conditions.

The effect of the sensor fault on the formation behavior can be observed in Figure 9. In the absence of fault compensation, the sensor malfunction in UGV_1 introduces deviations in the synchronization errors, affecting the ability of the UGVs to maintain coordinated motion with respect to the leader. Once the fault is removed, the synchronization errors gradually converge toward zero. During the fault interval from $t = 30$ s to $t = 60$ s, the synchronization errors exhibit noticeable deviations due to the corrupted sensor measurement. Once the fault is removed at $t = 60$ s, the errors gradually decrease and converge toward zero, indicating the recovery of the synchronized behavior under fault-free operating conditions.

Figure 10 shows the impact of the sensor fault on the relative distances among the UGVs, defined according to (40). During the fault interval, the erroneous sensor measurements affect the coordination of the formation, causing noticeable deviations from the desired relative distances. Consequently, the follower UGVs are unable to accurately maintain their prescribed positions with respect to the leader, resulting in a temporary degradation of the formation configuration. In particular, the relative distance errors increase during $30\,\text{s} \leq t \leq 60\,\text{s}$ due to the sensor fault. Once the fault disappears, these errors gradually decrease and converge to zero.

Figure 11 presents the FE results associated with the sensor of UGV_1. During the initial transient response, the observer requires a short convergence period to adapt to the system dynamics and measurement conditions. Once the sensor fault is introduced, the estimated fault signal follows the actual fault behavior with good agreement throughout the faulty

interval. After the fault is removed, the estimation gradually returns to zero. These results demonstrate the capability of the proposed PI observer to reconstruct the sensor fault and provide reliable information about its magnitude and temporal evolution.

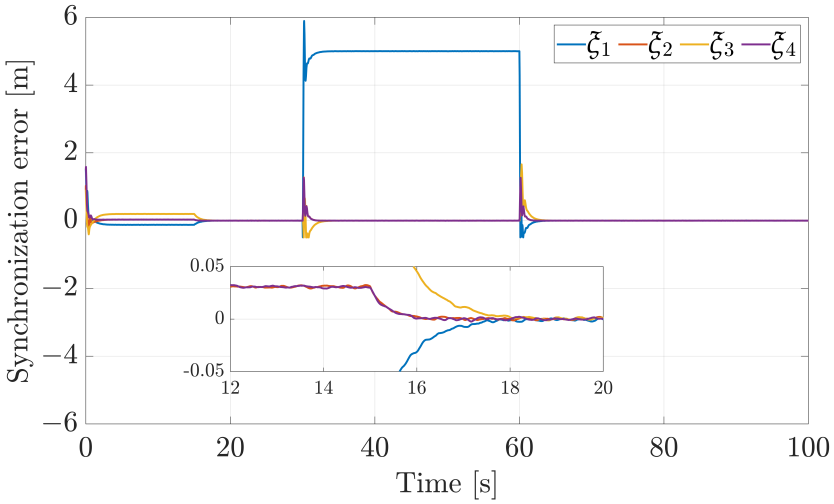

Figure 9. Synchronization error between the leader UGV and the follower UGVs under sensor fault conditions.

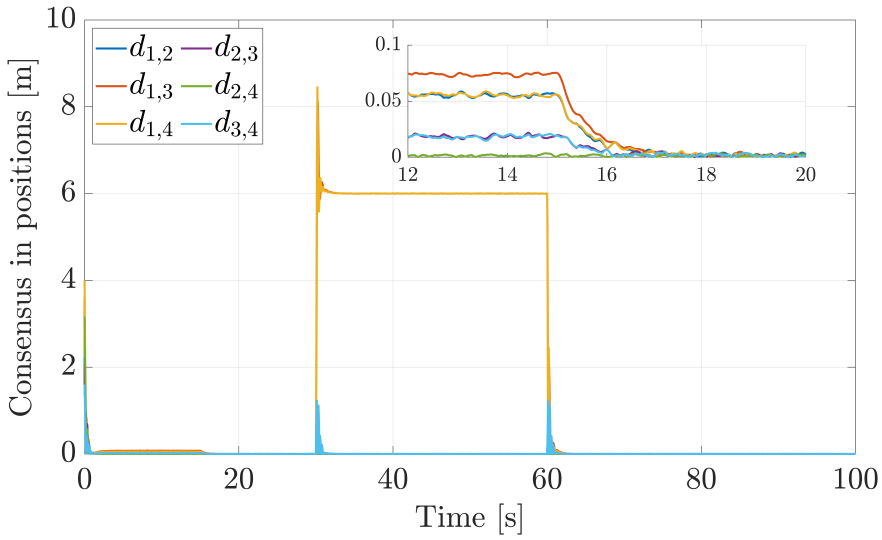

Figure 10. Relative distances among the UGVs under sensor fault conditions.

Figure 12 shows the control inputs u_x and u_y applied to the ground vehicles during the simulation. When the sensor fault occurs, a noticeable variation in the u_x control input is observed as a consequence of the affected measurement used by the observer-based control scheme. This effect is reflected as a transient deviation from its nominal behavior. Once the sensor fault is removed, u_x exhibits a second transient variation and subsequently converges toward its nominal fault-free value. This behavior illustrates the influence of the sensor fault on the control action and the recovery of the closed-loop system after the fault disappears.

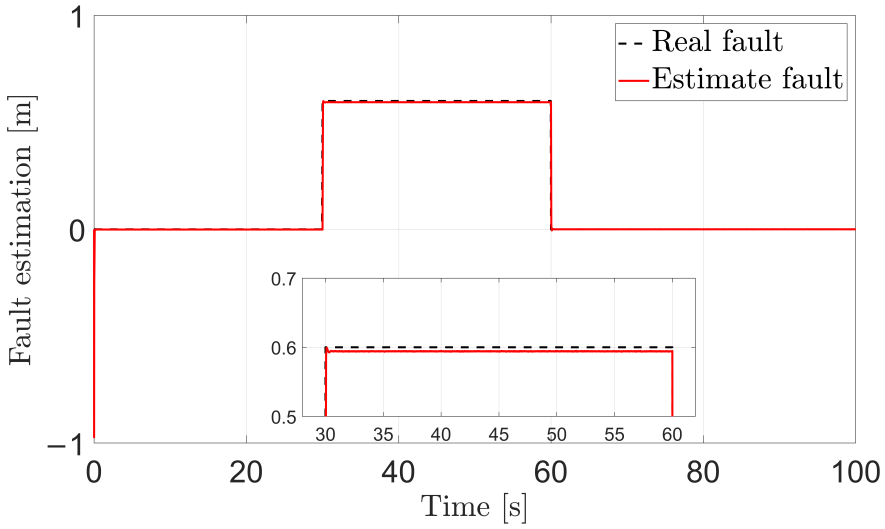

Figure 11. Sensor FE for UGV_1 in the faulty case.

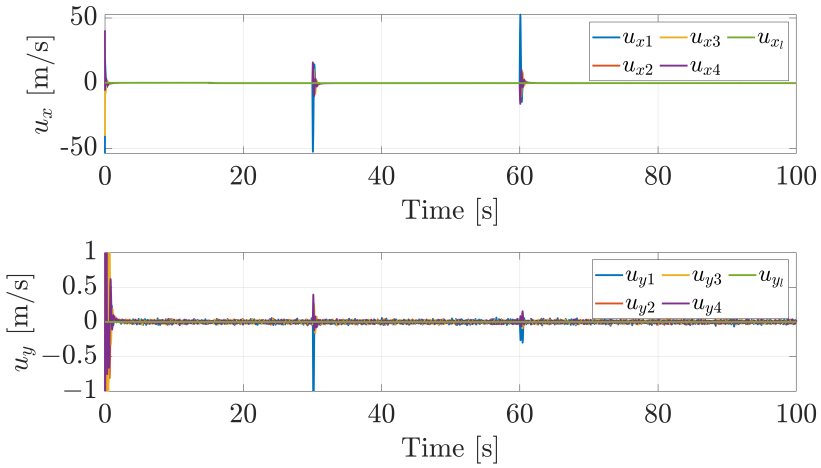

Figure 12. Control inputs fault case.

Although the control inputs u_x and u_y are generated in the inertial coordinate frame, their effect on the physical motion of the ground vehicle can be determined through the vehicle kinematics. Therefore, these control signals are transformed into the longitudinal and angular velocities of each vehicle by means of the inverse Jacobian matrix $J_p^{-1}(\theta_i)$, as follows:

$$\begin{bmatrix} v_{x_i} \\ \omega_i \end{bmatrix} = J_p^{-1}(\theta_i) \begin{bmatrix} u_{x_i} \\ u_{y_i} \end{bmatrix}, \tag{42}$$

where

$$J_p^{-1}(\theta_i) = \begin{bmatrix} \cos(\theta_i) & \sin(\theta_i) \\ -\frac{1}{l_r}\sin(\theta_i) & \frac{1}{l_r}\cos(\theta_i) \end{bmatrix}. \tag{43}$$

The resulting longitudinal and angular velocities are subsequently used to determine the front-wheel steering angle according to the Ackermann steering relation (31). Hence, the control actions generated by the proposed leader-following consensus strategy are ultimately translated into the longitudinal motion and steering commands required by each ground vehicle. Consequently, variations in u_{x_i} and u_{y_i}, including the transient variations associated with the occurrence and removal of the sensor fault, are propagated through the kinematic transformation and reflected in the steering action of the vehicle.

6. Conclusions

This paper addresses distributed sensor FE in leader-following multi-agent systems with UGVs. A distributed PI observer is developed to reconstruct each agent's augmented state and estimate sensor faults using only local measurements and neighbor-shared information. The sensor fault problem is reformulated as an equivalent actuator fault problem, and the observer is embedded into a leader-following consensus scheme, yielding a unified formulation for synchronization and estimation errors. The approach is validated in a cooperative formation scenario using a kinematic model. Under fault-free conditions, state reconstruction and formation errors converge to zero. Under sensor faults, performance degrades temporarily, but the PI observer accurately estimates the fault signal, which returns to nominal once the fault disappears. The simulation results demonstrate the ability of the proposed PI observer to estimate sensor faults in MASs. The current stability conditions are derived for a fixed and undirected communication topology. Extending the proposed framework to directed, switching, or time-varying graphs would require reformulating the stability analysis to account for topology-dependent properties and changes in the communication graph, which is considered as a direction for future research. Future work includes active fault-tolerant control for sensor faults, simultaneous actuator and sensor faults, switching/time-varying topologies, and experimental validation on a physical vehicle fleet.

Author Contributions: Conceptualization, J.A.V.T. (Jesus A. Vazquez Trejo) and E.P.-C.; methodology, J.A.V.T. (Jesus A. Vazquez Trejo) and A.D.E.P.; software, J.A.V.T. (Jesus A. Vazquez Trejo), A.D.E.P., E.P.-C. and J.A.V.T. (Juan A. Vazquez Trejo); validation, J.A.V.T. (Jesus A. Vazquez Trejo); formal analysis, E.P.-C., J.F.G.-C. and M.A.-M.; investigation, E.P.-C.; writing—original draft preparation, A.D.E.P., J.F.G.-C., M.A.-M. and J.A.V.T. (Juan A. Vazquez Trejo); writing—review and editing, A.D.E.P., J.F.G.-C., M.A.-M. and J.A.V.T. (Juan A. Vazquez Trejo); visualization, J.A.V.T. (Jesus A. Vazquez Trejo); supervision, J.A.V.T. (Jesus A. Vazquez Trejo), J.F.G.-C., M.A.-M. and J.A.V.T. (Juan A. Vazquez Trejo); project administration, M.A.-M. All authors have read and agreed to the published version of the manuscript.

Funding: This research was funded by Tecnológico Nacional de México un- der the program Proyectos de Investigación Científica, Humanística, de Desarrollo Tecnológico e Innovación.

Data Availability Statement: The original contributions presented in this study are included in the article. Further inquiries can be directed to the corresponding authors.

Conflicts of Interest: The authors declare no conflicts of interest.

References

1. Rizk, Y.; Awad, M.; Tunstel, E.W. Cooperative heterogeneous multi-robot systems: A survey. *ACM Comput. Surv. CSUR* **2019**, *52*, 1–31. [CrossRef]
2. Kwa, H.L.; Kit, J.L.; Bouffanais, R. Balancing Collective Exploration and Exploitation in Multi-Agent and Multi-Robot Systems: A Review. *Front. Robot. AI* **2022**, *8*, 771520. [CrossRef] [PubMed]
3. Li, X.; Wang, S.; Zeng, S.; Wu, Y.; Yang, Y. A survey on LLM-based multi-agent systems: Workflow, infrastructure, and challenges. *Vicinagearth* **2024**, *1*, 9. [CrossRef]
4. Kamel, M.A.; Yu, X.; Zhang, Y. Formation control and coordination of multiple unmanned ground vehicles in normal and faulty situations: A review. *Annu. Rev. Control* **2020**, *49*, 128–144. [CrossRef]
5. Lujak, M.; Giordani, S.; Omicini, A.; Ossowski, S. Decentralizing coordination in open vehicle fleets for scalable and dynamic task allocation. *Complexity* **2020**, *2020*, 1047369. [CrossRef]
6. Wang, J.; Zhang, J. Active Fault-tolerant Control Research of Multi-Agent System. *J. Phys. Conf. Ser.* **2021**, *1754*, 012088. [CrossRef]
7. Zhang, J.; Chen, Z.; Zhang, H.; Feng, T. Coupling effect and pole assignment in trajectory regulation of multi-agent systems. *Automatica* **2021**, *125*, 109465. [CrossRef]
8. Nguyen, N.P.; Pitakwatchara, P. Attitude Fault-Tolerant Control of Aerial Robots with Sensor Faults and Disturbances. *Drones* **2023**, *7*, 156. [CrossRef]

9. Caliskan, F.; Hacizade, C. Sensor and Actuator FDI Applied to an UAV Dynamic Model. *IFAC Proc. Vol.* **2014**, *47*, 12220–12225. [CrossRef]
10. Huang, T.; Pan, H.; Sun, W. A sensor fault detection, isolation, and estimation method for intelligent vehicles. *Control Eng. Pract.* **2023**, *139*, 105620. [CrossRef]
11. Sun, Y.; Li, H. An estimation method for sensor faults based on observer in interconnected systems. *PLoS ONE* **2024**, *19*, e0296848. [CrossRef] [PubMed]
12. Zhao, S.; Li, K.; Ahn, C.; Huang, B.; Liu, F. Tuning-Free Bayesian Estimation Algorithms for Faulty Sensor Signals in State-Space. *IEEE Trans. Ind. Electron.* **2023**, *70*, 921–929. [CrossRef]
13. Witczak, M.; Pazera, M.; Majdzik, P.; Matysiak, R. Development of A Guaranteed Minimum Detectable Sensor Fault Diagnosis Scheme. *Int. J. Appl. Math. Comput. Sci.* **2024**, *34*, 409–423. [CrossRef]
14. Chen, L.; Zhao, Y.; Fu, S.; Liu, M.; Qiu, J. Fault Estimation Observer Design for Descriptor Switched Systems With Actuator and Sensor Failures. *IEEE Trans. Circuits Syst. I Regul. Pap.* **2019**, *66*, 810–819. [CrossRef]
15. Yang, G.; Rezaee, H.; Serrani, A.; Parisini, T. Sensor Fault-Tolerant State Estimation by Networks of Distributed Observers. *IEEE Trans. Autom. Control* **2022**, *67*, 5348–5360. [CrossRef]
16. Doostmohammadian, M.; Meskin, N. Sensor Fault Detection and Isolation via Networked Estimation: Full-Rank Dynamical Systems. *IEEE Trans. Control Netw. Syst.* **2020**, *8*, 987–996. [CrossRef]
17. Han, W.; Trentelman, H.; Wang, Z.; Shen, Y. Distributed fault estimation for linear systems with actuator faults. *Int. J. Robust Nonlinear Control* **2020**, *30*, 6853–6878. [CrossRef]
18. Zhang, Z.; Li, Y.; Dong, J. Intermediate Observer-Based Robust Distributed Fault Estimation for a Complex Network of Dynamical Systems. *IEEE Trans. Autom. Sci. Eng.* **2024**, *21*, 5311–5319. [CrossRef]
19. Rahimi, F.; Ahmadpour, S. Neighborhood-based distributed robust unknown input observer for fault estimation in nonlinear networked systems. *IET Control Theory Appl.* **2022**, *16*, 972–984. [CrossRef]
20. Ye, Z.; Yu, Z.; Cheng, Y.; Jiang, B. Finite-time sliding-mode observer based distributed robust fault tolerant control for multi-agent systems against actuator and sensor faults. *Int. J. Syst. Sci.* **2023**, *55*, 618–630. [CrossRef]
21. Liang, D.; Ren, Y.; Lv, Y.; Wang, S. Robust Distributed Observers for Simultaneous State and Fault Estimation over Sensor Networks. *Sensors* **2024**, *24*, 7589. [CrossRef] [PubMed]
22. Farrera, B.; López-Estrada, F.; Chadli, M.; Valencia-Palomo, G.; Gómez-Peñate, S. Distributed Fault Estimation of Multi–Agent Systems Using a Proportional–Integral Observer: A Leader–Following Application. *Int. J. Appl. Math. Comput. Sci.* **2020**, *30*, 551–560. [CrossRef]
23. Xia, J.; Jiang, B.; Zhang, K. Resilient observer design of sensor fault estimation for discrete-time multi-agent systems: A distributed approach. *Int. J. Robust Nonlinear Control* **2021**, *31*, 9604–9618. [CrossRef]
24. Liu, C.; Yu, Z.; Patton, R.J. Decentralized fault estimation and distributed fault-tolerant tracking control co-design for sensor faulty multi-agent systems with bidirectional couplings. *Int. J. Control Autom. Syst.* **2023**, *21*, 810–819. [CrossRef]
25. Kheloufi, H.; Zemouche, A.; Bedouhene, F.; Boutayeb, M. On LMI conditions to design observer-based controllers for linear systems with parameter uncertainties. *Automatica* **2013**, *49*, 3700–3704. [CrossRef]
26. Chen, J.; Zhang, W.; Cao, Y.Y.; Chu, H. Observer-based consensus control against actuator faults for linear parameter-varying multiagent systems. *IEEE Trans. Syst. Man Cybern. Syst.* **2016**, *47*, 1336–1347. [CrossRef]
27. Martínez-Ramírez, L.A.; Vásquez-Cruz, R.I.; Munoz-Hernandez, G.A.; Mino-Aguilar, G.; Guerrero-Sánchez, W.F.; Ambrosio-Lázaro, R.C.; Guerrero-Castellanos, J.F. Trajectory Control for Car-like Mobile Robots via Frugal Predictive Control with Integrated Disturbance Rejection. *Actuators* **2026**, *15*, 260. [CrossRef]

Disclaimer/Publisher's Note: The statements, opinions and data contained in all publications are solely those of the individual author(s) and contributor(s) and not of MDPI and/or the editor(s). MDPI and/or the editor(s) disclaim responsibility for any injury to people or property resulting from any ideas, methods, instructions or products referred to in the content.